2016-07-17

In Vitro Monitoring of Time and Dose Dependent Cytotoxicity of Aminated Nanoparticles using Raman Spectroscopy

Esen Efeoglu
Technological University Dublin

Alan Casey
Technological University Dublin, alan.casey@tudublin.ie

Hugh Byrne
Technological University Dublin, hugh.byrne@tudublin.ie

Recommended Citation

Efeoglu, E. Casey, A. & Byrne, H.J. (2016) In vitro Monitoring of Time and Dose Dependent Cytotoxicity of Aminated Nanoparticles using Raman Spectroscopy", *Analyst,* 141, 5417-5431 (2016),

In vitro Monitoring of Time and Dose Dependent Cytotoxicity of Aminated Nanoparticles using Raman Spectroscopy

Esen Efeoglu[1,2,*], Alan Casey[2], Hugh J. Byrne[2]

[1]School of Physics, Dublin Institute of Technology, Kevin Street, Dublin 2, Ireland

[2]FOCAS Research Institute, Dublin Institute of Technology, Kevin Street, Dublin 2, Ireland

*Corresponding Author: esen.efeoglu@mydit.ie

Abstract

Investigation of possible adverse health effects of nanomaterials, in a rapid multi-parametric fashion, has become increasingly important, due to their increased production and potential uses in a wide range of application areas, from cosmetics to pharmaceutics. Although conventional *in-vitro* cytotoxicological techniques provide valuable information about the particle toxicity, the importance of gaining high content information in a single assay with the analysis of multiple parameters in a non-invasive and label-free way is still one of the biggest challenges in nanotoxicology. As a vibrational spectroscopic technique, the power of Raman spectroscopy for the analysis of cells, tissues and also nanoparticle localization within cells has been shown previously. In this study, the ability of Raman spectroscopy to fingerprint the dose and time dependent cellular responses and effect of cytotoxic events on biochemical constituents of the cells is monitored. A549 human lung carcinoma cells and aminated polystyrene nanoparticles (PS-NH_2) are used as a model cell line and nanoparticle, respectively. Following the determination of cellular responses in the presence of toxic PS-NH_2 by using conventional cellular assays, Alamar Blue (AB) and (3-(4,5-Dimethylthiazol-2-

yl)-2,5diphenyltetrazoliumbromid (MTT), and calculation of EC_{50} values for both assays, Raman spectroscopy was employed at response related doses and time points. Multiple point spectra from the cytoplasm, nucleus and nucleolus of 20 cells were acquired using Raman spectroscopy for each exposure dose and timepoint. Unsupervised principle components analysis (PCA) was applied to the Raman data sets for the comparison of exposed and unexposed cells as well as different exposure doses and times. The study shows the ability of Raman spectroscopy to provide information about cellular responses at different particle concentrations and exposure times with the aid of multivariate analysis. In the chosen range of concentrations, the most significant changes were observed in the cytoplasm for both time dependent and dose dependent cases due to the route of endocytosis The Raman spectral markers for lipidosis, ROS formation and oxidative stress related biochemical damage are determined and correlated with exposure dose and time, and the responses are correlated with conventional cytotoxicity assays.

Keywords: Nanotoxicology, Raman spectroscopy, aminated polystyrene nanoparticles, *in vitro* screening, dose-dependent toxicity, time-dependent toxicity, Label free imaging

Introduction

The growing interest and research in nanoscience and nanotechnology has introduced a plethora of nanomaterials into human life. More than 1600 products of nanotechnology have already found their place in the market, ranging from cosmetics to pharmaceutics (more information about nanotechnology based products can be found at http://www.nanotechproject.org/)[1]. From their production, to use and disposal by consumers, nanomaterials interact with living systems and the environment via different exposure routes. Due to their size, different surface properties and reactivity, related to their physicochemical properties, these novel materials can easily interact with biological systems. The emergence of Nanoscience and Nanotechnology has therefore given rise to the fields of Nanotoxicology[2] and Nanomedicine[3]. Nanotoxicology mainly deals with the possible adverse biological effects of nanomaterials for humans and ultimately the environment[4]. The Organisation for Economic Co-operation and Development (OECD) recommends established and commonly used protocols for nanotoxicological assessment[5], such as cell viability tests (3-(4,5-Dimethylthiazol-2-yl)-2,5diphenyltetrazoliumbromid (MTT), Neutral Red (NR) and Alamar Blue (AB)). On the other hand, Nanomedicine promises new paradigms in targeted drug delivery, diagnostics and imaging[6,7]. However, direct visualisation of the nanomaterials within cells, and the resultant cellular responses remains a challenge.

Raman spectroscopy has origin in inelastic collision of photons with molecules and provides fingerprint information about the specimen under investigation[8,9]. Due to the nature of the technique, fingerprint information at a molecular level, easy sample preparation steps, narrow spectral bandwidth and minimal influence from the water, a natural component of biological samples, the technique has attracted interest for the analysis of biological structures. The applicability of Raman spectroscopy as a tool for analysis of cells, tissues and biofluids has been demonstrated in recent years[10-15]. The technique has also been widely used for the

analysis of cell-drug and cell-nanoparticle interactions at a sub-cellular level[16-23]. The study of Dorney et al. demonstrated the ability of Raman spectroscopy to identify and discriminate different subcellular regions as well as the presence of the nanoparticles within these regions[14]. Moreover, the study of Keating et al. demonstrated the importance of multivariate analysis techniques on huge Raman data sets to gain further information about cell-nanoparticle localisation[24]. Also, the ability of the Raman spectroscopy to differentiate different cellular compartments, such as endosomes and lysosomes, as well as localisation of the nanoparticles in these compartments has been demonstrated[15]. For the case of Carbon Nanotubes, Knief et al.[25] probed the correlation of Raman biospectroscopic markers with conventional cytotoxicity assays, indicating that Raman spectroscopy can potentially be employed as a single, label free assay to localise nanoparticles, identify trafficking mechanisms and evaluate nanoparticle toxicity. However, an extensive study of dose and time dependent cellular responses to nanoparticle exposure has not as yet been reported.

The toxicity of aminated PSNPs (PS-NH_2) has been extensively studied by different research groups to determine the mode of interaction of these nanoparticles with different types of human cell lines by using conventional cytotoxic and microscopic techniques[26-31]. Polystyrene nanoparticles are taken up by most of the cell lines through endocytosis, which is accepted as the primary mechanism for nanomaterial uptake into the cells[32]. Basically, particles are taken up across the cell membrane by the formation of early endosomes which carry the nanoparticles to the lysosomes. After particles are engulfed by lysosomes, they are carried to the endoplasmic reticulum[15,33,34]. In the case of PS-NH_2, exposure of cells to the nanoparticles can induce toxicity due to the formation of Reactive oxygen species (ROS). The formation of ROS starts with the endocytosis of nanoparticles and continues throughout their trafficking within cells. The resultant oxidative stress causes the release of inflammatory factors and triggers apoptosis. Also, release of cationic nanoparticles into the cytosol due to

endosomal or lysosomal rupture resulting from membrane damage allows nanoparticles to reach the mitochondria and cause a change in mitochondrial membrane potential, also initiating the apoptotic process[29]. Aminated polystyrene particles induce cytotoxicity by triggering caspase mediated apoptotic pathways, even at low exposure doses, due to their cationic properties. Basically, pro-apoptotic Bcl-2 proteins are located on the mitochondrial membrane and cause the formation of holes which will release apoptogenic factors and trigger the caspase activity[26,29,30,35]. As the responses of cells to commercially available PS-NH_2 exposure *in vitro* have been extensively documented, they can serve as ideal model nanoparticles to explore the capabilities of Raman spectroscopy to monitor cellular responses.

In this study, the dose and time dependent cellular responses and effect of cytotoxic events on biochemical constituents of the cells are monitored using Raman spectroscopy. Aminated polystyrene nanoparticles (PS-NH_2) are chosen as model nanoparticles due to their well-documented cytotoxic mechanisms. Human lung adenocarcinoma (A549) cells were chosen for consistency with other studies[15,26], which show common modes of action in a number of cell lines, and as they act as models for human exposure by inhalation. Cells were exposed to PS-NH_2 in different doses and for different exposure times. In order to determine toxic effects of the PS-NH_2 in A549 cells, the conventional cytotoxic assay, Alamar Blue was carried out for 4, 8, 12 and 24 hr particle exposure. The 3-(4,5-dimethylthiazol-2-yl)-2,5-diphenyltetrazolium bromide (MTT) assay was also used to determine cytotoxic effect of PS-NH_2 in A549 cells after 8 hr particle exposure to compare the responses from different cytotoxicity assays. A549 cells were exposed to 2.5, 5 and 10 μM concentrations of the PS-NH_2 for the evaluation of spectroscopic signatures of the dose-dependent toxic responses in the fingerprint region of the Raman spectrum. Also, cells were exposed to 2.5 μM of PS-NH_2 for 4, 8, 12 and 24 hrs for the assessment of toxicity related changes in biomolecules such as the proteins, lipids and nucleic acids. In order to elucidate the roles of different cellular

regions and related toxic responses, Raman spectra were acquired from cytoplasm, nucleus and nucleolus. Raman datasets and unsupervised Principal Component analysis (PCA) was used for the elucidation and comparison of dose and time dependent biomolecular changes in the cells upon nanoparticle exposure.

Materials and Methods

Nanoparticles

100 nm amine-modified and fluorescently labelled, latex type, polystyrene nanoparticles (PS-NH_2, Product Number: L9904) were chosen as model nanoparticles for this study and purchased from Sigma-Aldrich (Ireland). The peak excitation and emission wavelengths of the PS-NH_2 are specified by the manufacturer as 481 and 644 nm, respectively. The PS-NH_2 were further characterised using a Malvern Zetasizer ZS to determine their size and surface potential in phosphate buffered saline (PBS) and cell culture medium. The nanoparticles were freshly prepared in pre-warmed cell culture medium containing supplements on the day of exposure.

Cell Culture

The human lung adenocarcinoma cell line, A549, was purchased from ATCC (ATTC. No: CCL-185) and cultured in Dulbecco's Modified Eagle's Medium Nutrient Mixture F-12 HAM (DMEM-F12) supplemented with 2mM L-glutamine and 10% foetal bovine serum (FBS, Sigma Aldrich) at 37 ^{o}C in a humidified 5% CO_2 incubator. Cells were sub-cultured at three days intervals to 60%-70% confluency.

Preparation of nanoparticle solutions

The PH-NH_2 solutions for both Raman measurements and cytotoxicity assays were prepared to the desired concentrations from initial concentrations by diluting the nanoparticles directly in 10% FBS and 2mM L-glutamine supplied DMEM-F12.

Cytotoxicity Assays and Determination of half-maximal effective concentration (EC_{50})

Alamar Blue (AB) and 3-(4,5-dimethylthiazol-2-yl)-2,5-diphenyltetrazolium bromide (MTT) assays were used to evaluate dose and time dependent cytotoxicity responses of 100 nm PS-NH_2 in A549 cells. AB and MTT assays were purchased from Biosciences Ltd(IRL) and Sigma-Aldrich (Dublin, Ireland), respectively and both assays were carried out on the same 96-well plate (Nunc, Denmark) by following manufacturer's instructions. A549 cells were seeded onto 96-well plates with densities of $1x10^5$ cells/mL and incubated at 37 ^oC in 5% CO_2 for 24 hrs for initial attachment and to achieve the desired confluency. PS-NH_2 solutions were prepared in the concentration range from 40 to 0.3125 μM by serial dilutions in pre-warmed DMEM-F12 medium supplemented with 10% FBS and 2mM L-glutamine. Following 24 hr initial attachment, the medium was removed and cells were rinsed with 100 μl/well PBS. A549 cells were exposed to the range of PS-NH_2 concentrations for each of the time points, 4, 8, 12, 24 and 48 hr. 10% Dimethyl sulfoxide (DMSO), prepared in cell culture medium, was used as a positive control. Six replicates of each different nanoparticle concentration, negative (A549 cells) and positive (DMSO) controls were used in each 96-well plate and 3 independent experiments were used to evaluate cytotoxic response of the PS-NH_2 on A549 cells for both assays. After particle exposures, the cell medium containing nanoparticles was removed and cells were washed with PBS three times. AB/MTT solution was prepared in the ratio of 5% [v/v] solution of AB and 10% [v/v] of MTT dye in un-supplemented DMEM-F12. A 100 μl/well of MTT/AB solution was added to A549 cells and they were incubated for 3 hrs at 37 ^oC in 5% CO_2. A microplate reader (SpectraMax-M3, Molecular Devices, USA) was used to measure AB fluorescence emission at 595 nm

(excitation/emission 540/595 nm, respectively). Following AB measurement, the cell medium containing AB and MTT is removed and cells were rinsed with PBS. 100 μl/well of DMSO were added to the 96-well plates and plates were agitated at 200 rpm for 10 mins. MTT absorbance was measured at 570 nm by using same plate reader system. The EC_{50} calculation was made by using a four parameter sigmoidal fit in SigmaPlot.

Raman Spectroscopy

Raman spectroscopy was used to monitor dose and time dependent changes of cellular constituents of A549 cells upon PS-NH_2 exposure. Approximately ~16000 cells per substrate were seeded onto CaF_2 disks and incubated for 24 hrs at 37 ^oC in 5% CO_2 for initial attachment. After initial attachment of the cells, cell medium was removed and cells were rinsed with PBS. The cell medium of A549 cells, which were used as control and will be referred to as unexposed cells throughout the study, was replaced with fresh 10% FBS and 2mM L-glutamine supplemented DMEM-F12. For the preparation of exposed cells, PS-NH_2 solutions with concentrations of 2.5, 5 and 10 μM were prepared in FBS and L-glutamine supplemented DMEM-F12 for the evaluation of dose dependent responses. A549 cells were exposed to the each concentration of PS-NH_2 for 8 hrs. Exposures to 2.5 μM PS-NH_2 were used for the assessment of time-dependent cellular responses, at 4, 8, 12, 24 and 48 hrs. In parallel, unexposed cells were incubated in fresh medium at 37 ^oC in 5% CO_2 for periods equivalent to the PS-NH_2 exposure times. Following the particle exposures and incubation of unexposed cells, medium containing PS-NH_2 for exposed cells and cell medium for unexposed cells was removed and cells were washed with PBS thrice. 10% formalin was used to fix cells for 10 mins. After fixation of cells, formalin was removed and cells were washed three times with distilled and sterilised water. Throughout the study, Raman measurements were acquired by using water-immersion objective. Therefore, after fixation and washing steps, cells were kept in water and spectra were acquired in water.

A Horiba Jobin-Yvon LabRAM HR800 spectrometer, equipped with a 785 nm diode laser as source was used throughout the study. All measurements were acquired in water by using a x100 water immersion objective (LUMPlanF1, Olympus, N.A. 1). The spectrometer was calibrated to the 520.7 cm^{-1} line of silicon prior to spectral acquisition. A 300 lines per mm grating was chosen, which provides approximately 1.5 cm^{-1} per pixel spectral dispersion. A 100 μm confocal pinhole was used for all measurements. The spectra were dispersed onto a 16 bit dynamic range Peltier cooled CCD detector. Point spectra from the cytoplasm, nucleus and nucleolus of 20 cells were acquired for each dose and exposure time. The spectral range from 400 to 1800 cm^{-1}, the so-called fingerprint region, was chosen and spectra were acquired for 2x30 seconds at each spot. Unexposed cells were used as control for comparisons of the different doses and exposure times.

Data Analysis

Raman data sets were transferred to Matlab (Mathworks, USA) for data analysis. Pre-processing was carried out in the same data analysis platform to improve spectral quality. For pre-processing, first, a mild smoothing was applied to data sets by using Savitsky-Golay filter (3^{rd} order and 9 points). Classical Least Squares (CLS) analysis was employed to minimize contributions from the background which is dominantly water in the immersion geometry[12,36]. Spectra were vector normalized following smoothing and background subtraction. Principle Component Analysis (PCA) was applied to pre-processed Raman data sets to differentiate the spectral changes in fingerprint region of the nucleus, nucleolus and cytoplasm upon PS-NH_2 exposure.

Results and Discussion

The well-established and commonly used cytotoxicity assay, AB, was carried out to determine the dose and time dependent toxic effect of PS-NH_2 on A549 cells[37-39]. Figure 1.I shows the plots of cytotoxic response of PS-NH_2 on A549 cells determined by the AB assay. Half-maximal concentration for cellular viability, EC_{50}, values relating to the different particle exposure times were calculated in SigmaPlot by a four parameter sigmoidal fit. For 4 hr PS-NH_2 exposure, the EC_{50} value was calculated to be 20±1 μM. After 12 hr particle exposure, the EC_{50} value was decreased to 11±4 μM. For 24 hr exposure of A549 cells to the PS-NH_2, a median cytotoxic effect at a concentration of 10±2 μM was observed, while when cells were exposed to the PS-NH_2 for 48 hrs, the EC_{50} value is calculated as 2.8±0.2 μM .The degree of toxicity is inversely related to the EC_{50}[40] and thus, when all exposure times are compared, the cytotoxicity of PS-NH_2 progressively increases from 4 hr to 48 hr exposure.

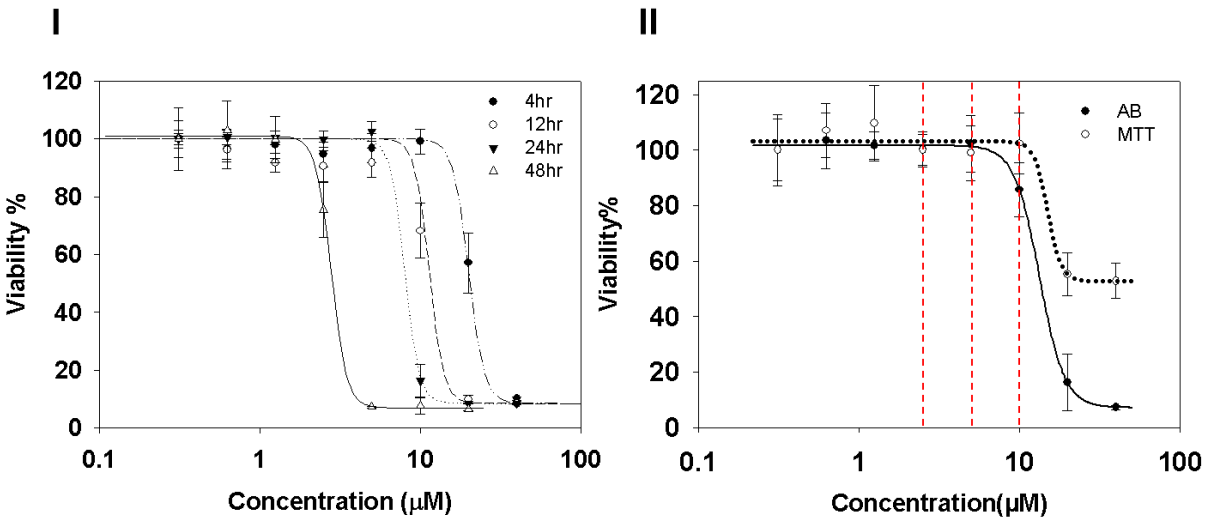

Figure 1. I) Cytotoxicity of 40 nm amine-modified polystyrene nanoparticles (PS-NH_2) after 4, 12, 24 and 48 hr exposures determined by the Alamar Blue assay. **II)** Cytotoxicity of 40 nm amine-modified polystyrene nanoparticles (PS-NH_2) after 8 exposure determined by the

Alamar Blue and MTT assays. The concentrations (2.5, 5 and 10μM) which are used throughout the study are indicated by red dashed lines. Data are expressed as % of control mean ± SD of three independent experiments.

As an alternative and complementary measure of cytoxic response, the MTT assay was also employed to monitor the toxic response of A549 cells to PS-NH_2 exposure. Figure 1.II compares the dose dependent responses for 8 hr PS-NH_2 exposure from the two assays, MTT and AB. EC_{50} values for both assays were observed similar to each other which are 13±1 and 15±5 μM for AB and MTT, respectively. Although EC_{50} values were calculated to be similar, the difference in the underlying mechanism of toxicity changes according to concentration of PS-NH_2. The increasing concentrations of PS-NH_2 cause a rapid decrease in cell viability when it is determined by the AB assay, compared to that which is determined by MTT after 8hr exposure. For this reason, significantly different toxicological profiles can be obtained from well-established cytotoxicity assays due to the limitations of specific colorimetric label based assays.

The dose and time dependent cytotoxic response of a cytotoxicological assay reflects a complex cascade of events, triggered by endocytosis of the nanoparticles, giving rise to subsequent oxidative stress, inflammatory responses, apoptosis and cell death, as described for example by Maher et al.[41]. Each cytotoxicity assay measures the toxic response of cells in different ways, and the relative sensitivity of the assay depends on the events in the cascade to which it is sensitive. AB is a measure of overall cellular activity as measured by the transformation of Rezazurin Sodium Salt (weak fluorescence) into Resofurin Sodium salt which has a strong fluorescence. Although the exact mechanism of the reduction reaction is unknown, as there are multiple cellular sites of conversion, AB assay provides valuable information about the overall activity of the cell population[38,39,42,43]. On the other hand, the MTT assay measures the cell activity based on formazan product formation which relates to

the mitochondrial activity of cells[44]. In cases such as cellular exposure to poly (amido amine) (PAMAM) dendrimer nanoparticles, in which endosomolysis leads to translocation of the nanoparticles to the mitochondria, MTT is seen to be significantly more sensitive than AB, which measures the subsequent change to the cytosolic activity[45]. The formation of ROS inside the cell is regulated by different factors such as protective enzymes and antioxidant mechanisms. The ROS formation and cell protection mechanism works through the cross-talk between cytosolic events and mitochondrial events upon the presence of ROS. In the case of PS-NH_2 exposure, the nanoparticles are trafficked from endosomes to lysosomes, and the toxic insult is first manifest through generation of ROS in the cytosol (around cell membrane and lysosomes), which subsequently impacts on the mitochondria[46,47].

Although cytotoxicity assays such as AB, Neutral Red, and those based on tetrazolium salts (MTT, MTS, WST-1), provide valuable information about the toxic effect of material the under investigation, these techniques are not a definitive measure of cell viability and provide little information about the mechanism of action of the toxicants in terms of molecular determinants and pathways. In contrast, as a label free technique, Raman spectroscopy can potentially provide a high content spectroscopic profile of the cells and complete biochemical response at a given exposure time and dose (as illustrated by the mean spectra of the subcellular regions of the unexposed cell population, Supplementary Figure S1). The dose dependent cytotoxicity measurements serve as a range finding test for Raman analysis.

Figure 2 shows the PCA of spectra corresponding to cytoplasm, nucleus and nucleolus of the 8hr unexposed control and 10 μM PS-NH_2 exposed cells. Although this dose is less than the EC_{50} for both assays at this time point, it induces a significant reduction in viability, as registered using the AB assay (Figure 1.II). Figure 2.I shows the scatter plots of PCA and the data sets relating to unexposed and exposed cells are indicated with closed circles and open circles, respectively and coded with colours according to the different cellular regions.

Cytoplasm, nucleus and nucleolus are indicated with red, green and blue, respectively. The same colour coding system is used for exposed cells, but with the use of open circles. The spectra corresponding to the nuclear areas (nucleus and nucleolus) and cytoplasm are clearly differentiated for both exposed and unexposed cells according to PC1, which represents the most significant variance (46%) among the data, originating from biochemical differences between the combined nuclear area and cytoplasm. The spectra relating to the cytoplasm of both exposed and unexposed cells score negatively according to Loading 1 ($PC1<0$), while nuclear and nucleolar spectra score positively according to Loading 1 ($PC1\geq0$). PC2 gives information about the second highest variance (16%) among the data sets, and differentiates each region for exposed and unexposed cells. For all cellular regions, exposed cells are clearly differentiated from unexposed cells, indicating that the spectral differences are larger than the intrinsic variability of each region, and score positively according to PC2 (indicated by open circles) while unexposed cells score negatively ($PC2<0$) (indicated by closed circles).

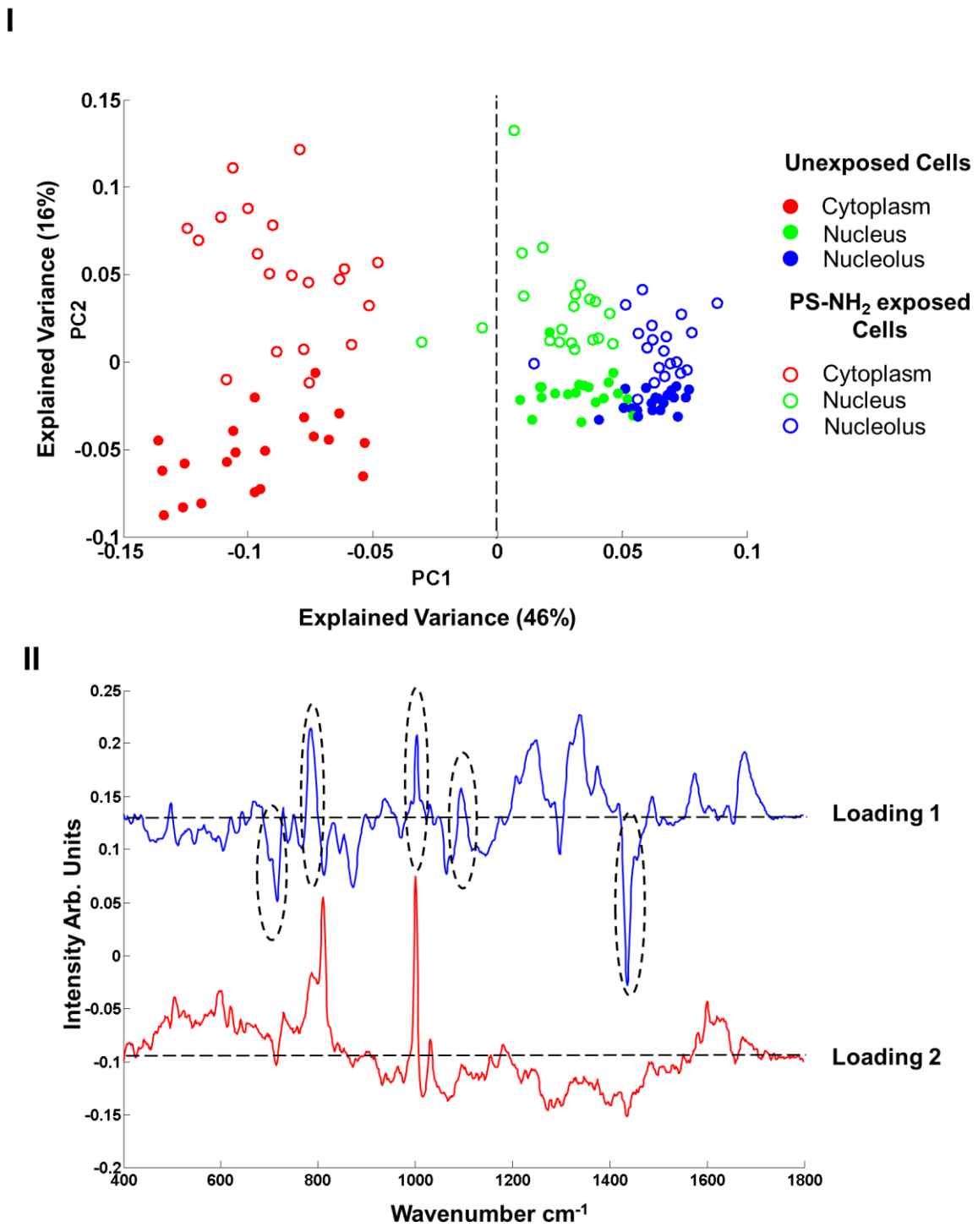

Figure 2. I) Scatter plot of the PCA of spectra corresponding to cytoplasm, nucleus and nucleolus of the (8hr) unexposed and PS-NH_2 exposed cells for 10 μM concentration of nanoparticles. Different cellular regions are coded as follows; red for cytoplasm, green for nucleus and blue for nucleolus. Exposed and unexposed cells are indicated by open circles

and closed circles, respectively. **II)** First 2 loadings of PC analysis; loadings are offset for clarity and the dotted line represents the zero '0' point for each loading. In loading 1, notable bands which are used to differentiate the nuclear region from cytoplasm are indicated by black dashed outlines.

Figure 2.II shows the first two loadings of the PCA, corresponding to all regions of exposed and unexposed cells. As seen in Figure 2.I, exposed and unexposed cells differentiate from each other based on the differences in biochemical composition of nuclear regions and cytoplasm according to PC1. The spectra of the nuclear area of the cell, which is composed of nucleus and nucleolus, score positively, while spectra corresponding to cytoplasm score negatively, according to PC1, for both exposed and unexposed cells. For this reason, the positive features of loading 1 are dominated by nuclear and nucleolar related bands, while negative features relate to the cytoplasm. The most dominant features which are used to differentiate the nuclear area (nucleus and nucleolus) and cytoplasm, the positive features at 785, 1003, 1094 cm^{-1} and the negative features ~ 719, 1437 cm^{-1}, are indicated with black outlines in Figure 2.II. Amongst the positive features, the bands at ~ 785 cm^{-1} (Nucleic acids uracil (U), thymine (T), cytosine(C) ring breathing modes in the DNA/RNA bases, O-P-O backbone), 1003 (phenylalanine(Phe)), 1094 cm^{-1} (DNA), 1248 cm^{-1} (Guanine(G) and cytosine (NH_2), Amide III), 1339 cm^{-1} (Phe, tyrosine(Tyr), nucleic acid), 1373 cm^{-1} T, G, adenine(A) bases of deoxyribonucleic acid (DNA) and ribonucleic acid (RNA)), 1575 cm^{-1} (G, A of nucleic acids) and 1678 cm^{-1} (bound or free NAHD, Amide I region) indicate the predominance of nucleic acids and proteins which are abundant in the nuclear area[48-50]. On the other hand, the dominant negative features include those at ~719 cm^{-1} (membrane phospholipid head, phosphatidylcholine), 873 cm^{-1} (hydroxyproline, tryptophan (Trp)), 1064 cm^{-1} (acyl chains, υ(C-C)), 1078 cm^{-1} (phospholipids), 1298 cm^{-1} (fatty acids) and 1437 cm^{-1} (Lipids, acyl chains, CH_2 deformation), which are more characteristic of the lipid rich

cytoplasm. Unexposed and exposed cells are differentiated mainly according to loading 2, as seen in Figure 2.II. Although there are some contributions to the loading 2 from PS-NH_2 in the positive features, cells exposed for 8 hr to 10 μM of PS-NH_2 are mainly differentiated from the unexposed cells by increases in the intensities of nucleic acid bands at 785 cm^{-1} and 810 cm^{-1} (RNA, O-P-O stretching) cm^{-1} and protein Amide I band at 1604 cm^{-1}. For loading 2, the bands derived from PS-NH_2 at 620, 1003, 1030 and 1600 cm^{-1} have been excluded from discussion.

Polystyrene nanoparticles are taken into the cells by the mechanism known as endocytosis. Previous studies have confirmed that the polystyrene nanoparticles (PS-COOH) are taken up into endosomes and carried to lysosomes[15,26,51-53]. Most of the nanoparticles are observed in lysosomes after 8 hr particle exposure. For this reason, after shorter exposure times, for example 8 hr, most of the cytotoxic responses can be attributed to changes in the cytoplasm and due to a cascade of processes including ROS formation, mitochondrial damage and lipidosis[26,41], but notably, the nucleus and nucleolus are not affected as much as cytoplasm. In order to better identify changes in the biomolecular composition of the cytoplasm, nucleus and nucleolus upon PS-NH_2 exposure, the mean spectra of particle exposed cells and unexposed cells were obtained and the spectral differences for each individual cellular region are evaluated by subtracting the mean spectra of exposed cells from the mean spectra of unexposed cells (Figure 3). When the mean spectra of cytoplasm, nucleus and nucleolus are analysed, the most significant changes are observed in the cytoplasm (red) of exposed cells compared to the corresponding control, as seen in Figure 3. For all cellular regions, some contributions from the PS-NH_2 are observed in PS-NH_2 exposed cells and the bands related to PS are highlighted with grey and excluded from band assignments.

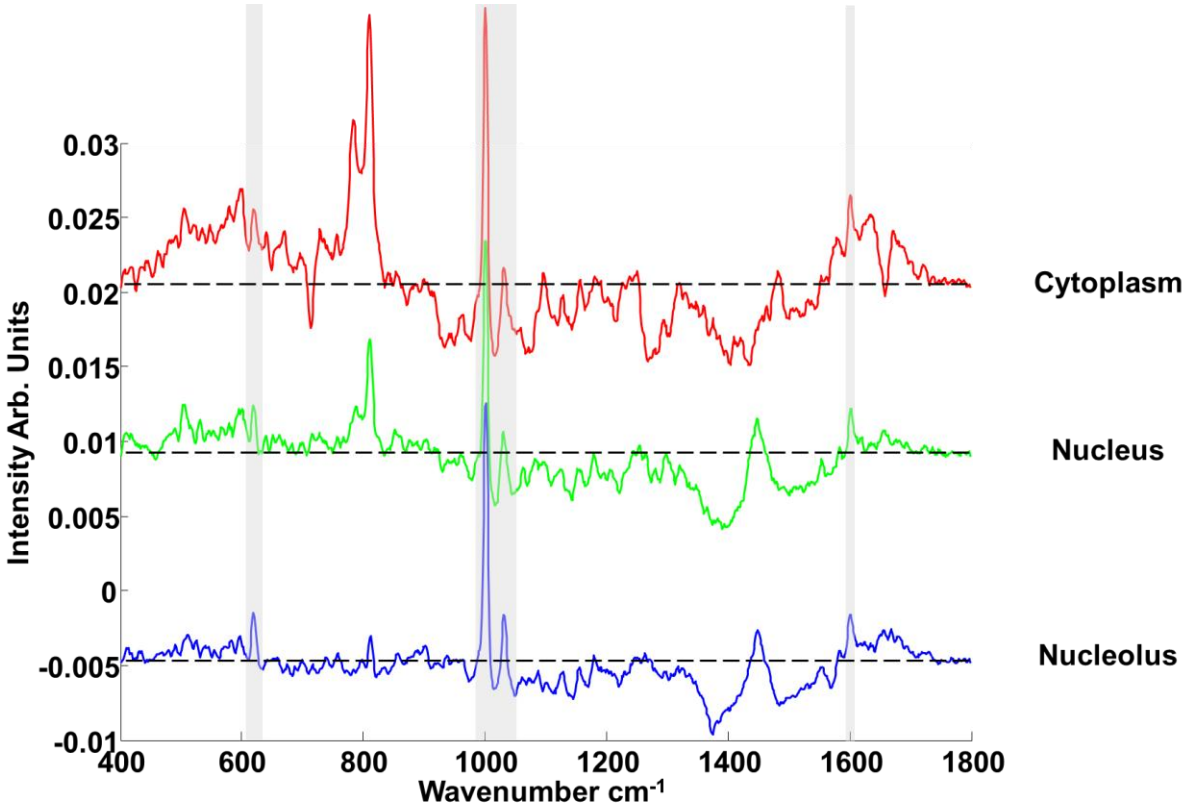

Figure 3. Mean difference spectra of cytoplasm (red), nucleus (green) and nucleolus (blue) obtained by subtraction of mean spectra of 8hr PS-NH_2 exposed cells from mean spectra of unexposed cells. The spectra are offset for clarity, the dashed line indicating the zero point. The bands related to PS are indicated with grey highlights.

Cellular events as a result of nanoparticle exposure to, and uptake of, a toxicant cause the production, consumption and/or damage of biochemical constituents inside the cells. The changes in the biochemical constituents are reflected in the Raman spectral data sets and can be used to identify different cellular events. When cells are exposed to 10 μM PS-NH_2 for 8 hr, the most significant changes are observed in the cytoplasm, as seen in Figure 3. The intensity of the bands at 785 and 810 cm^{-1} become significantly higher compared to the controls. The band at 785 cm^{-1} can be attributed to the ring breathing mode of nucleic acid bases (U, T and C) or O-P-O backbone stretching of nucleic acids, as so can be attributed to either RNA or DNA[46-48]. The band at 810 cm^{-1} is attributed to RNA structures[54,55] and relates

to asymmetric stretching of the sugar-phosphate diester. The presence of 785 and 810 cm^{-1} bands in Raman spectra of the cytoplasm has been examined in the study of Ghita et al.[56], which showed that an increase of the RNA bands during cell differentiation can be attributed to repressed translation of mRNAs and increasing amounts of noncoding RNAs in the cytoplasm. As seen in Figure 3, upon PS-NH_2 exposure, the band at 810 cm^{-1} shows a significant increase compared to its control with a concomitant increase in the band at 785 cm^{-1}, while control cells did not show any significant band at 810 cm^{-1} for cytoplasm (Supplementary Figure S2).

The exposure of cells to toxic PS-NH_2 is known to result in ROS formation[57]. Increased ROS levels in the cell first impacts on the mitochondria and causes the mediation of cytotoxic effects and release of pro-apoptotic factors with increasing production of mitochondrial ROS[58], which in turn can cause deformation of cytoplasmic RNAs which generally localises in close proximity to the mitochondria and results in repression of translation and accumulation of noncoding RNAs in the cytoplasm of exposed cells. The role of oxidative stress in the repression of mRNA translation has been shown previously[59-61]. For this reason, an increase in the intensity of the 810 cm^{-1} band in the cytoplasm can be attributed to changes in RNA content, as a result of oxidative stress and can be used as a mitochondrial damage marker in a label-free way. Although the band at 785 cm^{-1} can be attributed to either DNA or RNA, the concomitant increase in the 810 cm^{-1} for short exposure times is consistent with a primary attribution of increased RNA accumulation in cytoplasm.

The cytoplasmic responses upon particle exposure are further explored according to their correlation with the concentration of toxicant. The effect of PS-NH_2 exposure on A549 cells was also monitored using intermediate (5μM) and sub-lethal doses (2.5μM), for 8hrs. PCA clearly differentiates unexposed and exposed cells according to PC1 for all exposure doses.

Scatter plots of unexposed and exposed cells for each exposure dose are provided in Supplementary Figure S3, and a representative example of scatter plot of cytoplasm of exposed and unexposed cells for 10 μM PS-NH_2 is shown in Figure 4.I. The respective loadings for the cytoplasmic regions of 2.5, 5 and 10 μM are shown in Figure 4.II.

For 10 μM PS-NH_2, which is close to the EC_{50} value for AB, exposed cells are differentiated from unexposed cells due to a significant increase of the intensity of nucleic acid bands represented by positive features of loading 1 (785 and 810 cm^{-1}), which can also be seen in the difference of mean spectra of exposed and unexposed cells (Figure 3). Notably, the changes in this region are seen to evolve monotonically with exposure dose (Figure 4, Figure S4), confirming a direct correlation between the changes in nucleic acid spectral signatures and particle exposure.

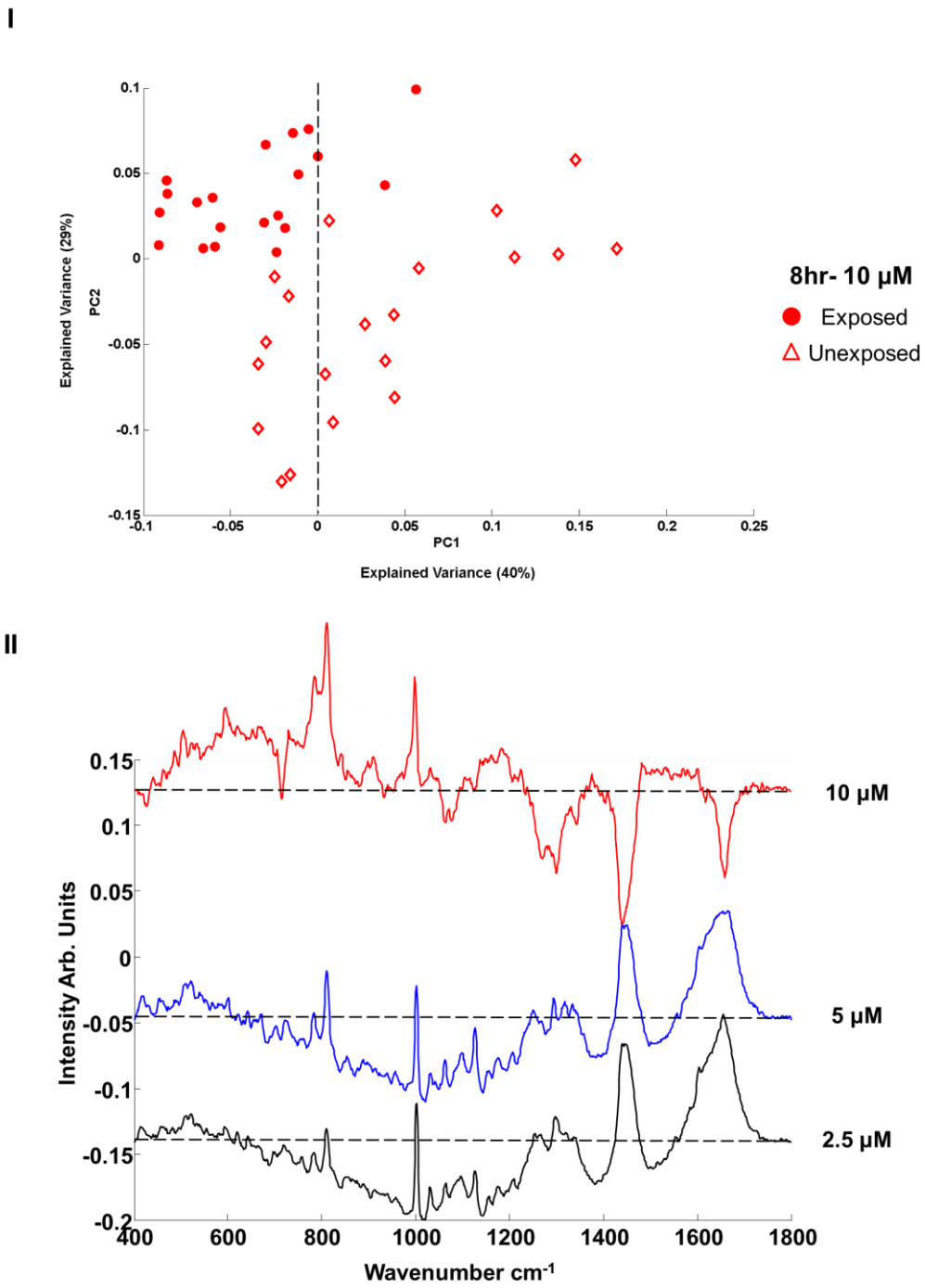

Figure 4. I) Scatter plot of the PCA of spectra corresponding to cytoplasm of the unexposed cells (closed circles) and cells exposed to 10 µM PS-NH_2 for 8 hr (open diamond). **II)** Loadings of PC1 for pairwise analysis of cytoplasm of exposed cells with the control for 10 µM (red), 5 µM (blue) and 2.5 µM (black) for 8 hr. The dotted line represents the zero '0' point for each loading. Loadings are offset for clarity.

Negative features of the loading (unexposed cells) are observed to be richer in protein and lipid content (bands at 1062, 1080, 1270, 1299 and 1438 cm^{-1}). The relatively higher amount of the lipids in unexposed cells compared to PS-NH_2 exposed cells can be attributed to damage of the lipidic structures such as lysosomes and membrane bounded cellular compartments upon PS-NH_2 exposure. When the nanoparticles are localised inside the lysosomes after 8 hrs, they become trapped due to the protonation of their surface in low lysosomal pH (~4.5). Protonation and the change in the lysosomal pH cause formation of a gradient for lipids to traffic into the lysosomes from the cytosol and finally the formation of enzymatically unbreakable complexes (Myeloid bodies)[26]. The lipid transfer from cytoplasm to lysosomes and accumulation of lipids in lysosomes, a phenomenon known as lipidosis, causes the loss of lipid related bands in the spectral profile of the cytoplasm. Moreover, later stages of lipidosis cause a distortion and rupture of the lysosomal membrane [62-65]. Therefore, changes in the intensities of the bands at 719 cm^{-1} (membrane phospholipids), 1270-1301 cm^{-1} (phospholipids, lipids), 1437 cm^{-1} (acyl chain of lipids) can be used to track lysosomal damage during nanotoxicological screening of toxic nanoparticles.

As seen in Figure 4, with the exception of the monotonic increase in the nucleic acid related bands at 785 and 810 cm^{-1}, sub lethal doses of PS-NH_2, result in significantly different spectral profiles compared to the cells exposed to 10 μM PS-NH_2. When the concentration of PS-NH_2 was reduced to 5 μM, the exposed cells show increased amounts of lipid, protein and nucleic acid in the cytoplasm compared to unexposed cells (the positive features of loading 1). Also, nucleic acid related bands are prominent at around 1095 cm^{-1} (PO_2^-), 1177 cm^{-1} (C, G) and 1292 cm^{-1} (C) , but are not evident in the 10 μM PS-NH_2 exposed cells. The 5 μM PS-NH_2 exposed cells also show increases in the intensity of protein (1030, 1208, 1250 and 1654 cm^{-1}) and lipid bands (1064 cm^{-1}), compared to unexposed cells. A similar PC Loading profile was observed when the dose was reduced to 2.5 μM, exhibiting a decrease in the

intensities of the bands at 785 cm^{-1} (Nucleic acids), 810 cm^{-1} (RNA), 1127 cm^{-1} (υ(C-N)), 1266 cm^{-1} (Amide III (α-helix)), 1319 cm^{-1} (G), 1333 cm^{-1} (G) and an increase in the intensity of the band at 1655 cm^{-1} (Amide I). When the respective loadings for each dose are compared, lipid and protein related bands are inverted in going from lethal (10 μM) to sub lethal (2.5 μM) PS-NH_2 doses. The change in the amount of lipid and protein structures with increasing dose can be related to damage of protein and lipid structures as a result of increasing amount of ROS inside the cell for toxic exposures.

Following the effect of dose of PS-NH_2 on A549 cells, the effect of exposure time was monitored by comparing particle exposed cells with their controls. In order to evaluate spectral differences progressively as a function of time, a sub lethal dose of PS-NH_2 (2.5 μM) was chosen and cells were exposed to the nanoparticles from 4 to 48 hrs. Figure 5.I shows the scatter plots of the PCA of spectra corresponding to cytoplasm of exposed and unexposed cells for 24 hr (2.5 μM), as a representative example of separation between exposed and unexposed cells. Scatter plots of cytoplasm of exposed and unexposed cells for each exposure time are provided in Supplementary Figure S5. As seen in Figure 5.I, for the case of 24 hr, exposed and unexposed cells are largely differentiated according to PC1 (Explained Variance 45%). Figure 5.II shows the comparison of the loadings of PC1 of cytoplasm of exposed and unexposed cells for 4, 8, 12, 24 and 48 hrs.

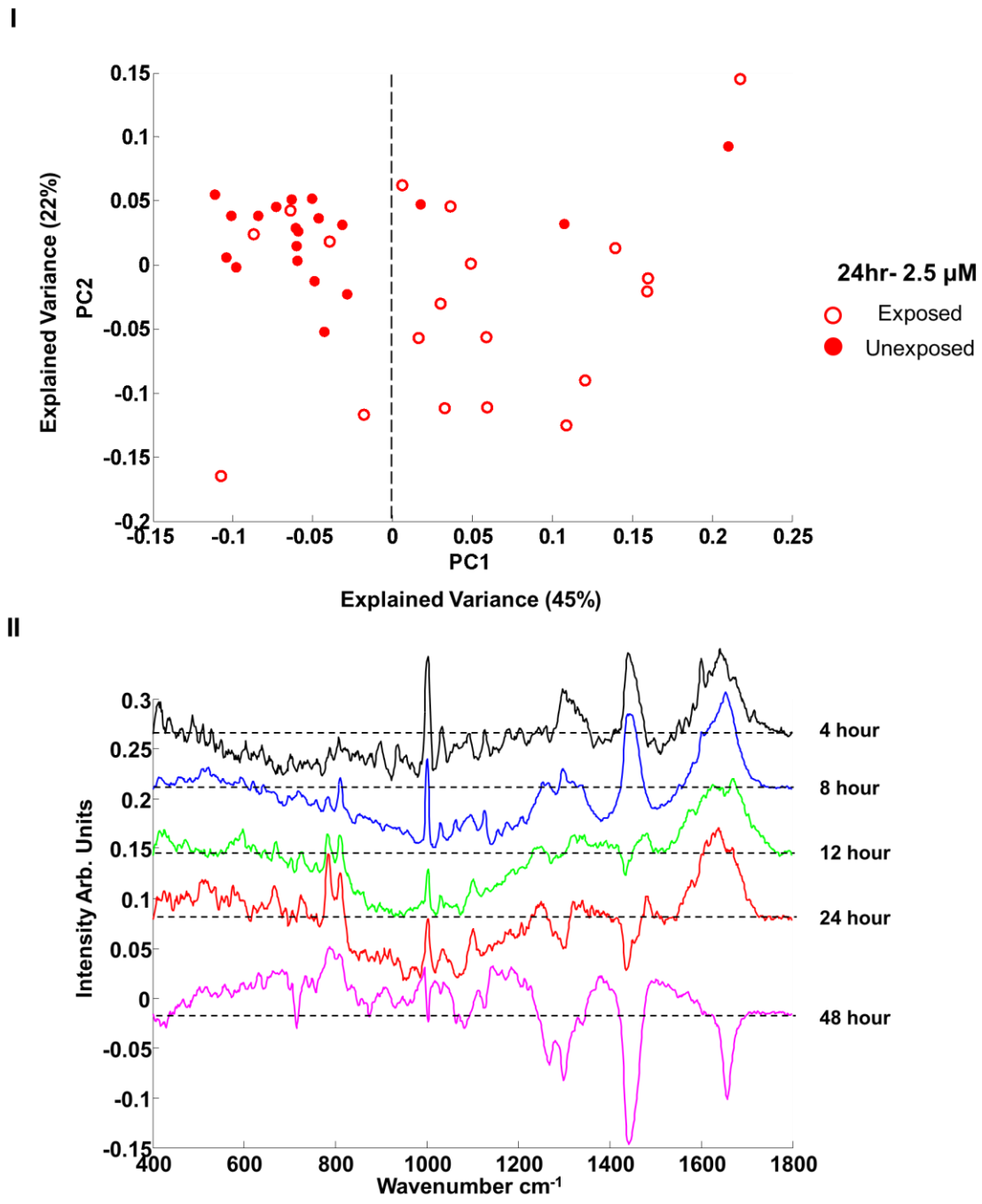

Figure 5. I) Scatter plot of the PCA of spectra corresponding to cytoplasm of the unexposed cells (close circles) and PS-NH_2 exposed cells (2.5 µM) (open circles) for 4, 8, 12 and 24 hr, **II)** Comparison of the Loading of PC1s for different PS-NH_2 concentrations (cytoplasm). 4, 8, 12, 24 and 48 hr are indicated with black, blue, green and magenta red, respectively. Positive features of the PCs are related to exposed cells while negative features of the PCs are

related to their controls. Loadings are offset for clarity. The dotted line represents the zero '0' point for each loading.

As in the case of the exposure dose dependent spectral profiles, the evolution of the nucleic acid features at 780 cm^{-1} and 810 cm^{-1} is observed to be prominent. However, these features are weak after 4 hr PS-NH_2 exposure, and the particle exposed cells differentiate from the unexposed cells largely due to their protein and lipid content. The bands at 1003 cm^{-1} (Phe), 1602 cm^{-1} (Phe) and 1640 cm^{-1} (Amide I) can be attributed to damaged protein structures resulting from the damage in the mRNA template and the distorted proteins accumulate inside the cell as well as normal proteins due to lysosomal damage[51]. The increasing intensity of the lipid bands at 1298 and 1440 cm^{-1} indicates an increasing amount of lipids in the cytoplasm due to increasing amount of endosomes and lysosomes upon PS-NH_2 exposure. When the time of exposure of the cells to the PS-NH_2 is increased to 8 hr, following the increases in protein and lipid bands, some changes start to occur in RNA accumulation in the cytoplasm due to the onset of repression of mRNA translation, which are manifest in the Raman spectra of PS-NH_2 exposed cells (positive features of loading 1) as an increase in the band at 810 cm^{-1}. An increase in the intensity of bands at 1319 (G) cm^{-1} and 1333 (G) cm^{-1} can also be observed with increasing exposure time. For this exposure time, the sharp band at 1602 cm^{-1}(Phe) disappears and the intensity of the 1003 cm^{-1} band reduces, which can be attributed to the onset of degradation of proteins.

After 12 hr exposure of A549 cells to PS-NH_2, more significant changes occur in the biochemical composition of particle exposed cells compared to previous exposure times. For this exposure time, as seen in Figure 5.II, the nucleic acid band at 785 cm^{-1} shows an increase in its intensity which indicates the increasing amount of nucleic acids in cytoplasm. Similar to the effect of dose, in the case of increased exposure time, the increase of nucleic acids in the cytoplasm can be observed at 810 cm^{-1} (RNA), with a larger increase in 785 cm^{-1} (RNA

and DNA) compared to 8 hr exposure. Although the increase in the 785 cm^{-1} band was attributed to RNA accumulation for shorter exposure times (up to 8 hr), an independent increase is observed on the 785 cm^{-1} band compared to 810 cm^{-1} with increasing exposure time, which can be attributed to an increase of DNA content in the cytoplasm. The increasing amount of DNA in the cytoplasm can be attributed to the decay of mitochondrial membrane and release of mitochondrial DNA into the cytoplasm, at this time point. ROS formation and mitochondrial decay affect the spectral profile of proteins and lipids in particle exposed cells and this is reflected in the Raman spectra of unexposed cells and causes the appearance of the bands at 1200-1300 cm^{-1} (Amide III) and 1438 cm^{-1} (Protein, Lipids) as negative features of PC1, which represent the unexposed cells. Also notable is the emergence in the loadings spectrum of bands at 1299 and 1438 cm^{-1}. They are both associated with lipid content inside the cytoplasm and the change in the intensity of the bands can be attributed to damage of lipidic structures due to lipidosis after PS-NH_2 exposure. The intensity changes in the 1438 cm^{-1} band can be further used determine cytotoxic events in the cytosol and damage of lysosomes. The band at 1299 cm^{-1} is progressively reduced until 12 hour particle exposure and becomes inverted for 24 and 48 hr particle exposure, which indicates that lipids are more abundant in unexposed cells compared to exposed ones. The intensity of the band at 1438 cm^{1} did not show any change up to 8 hr, but this band is inverted with increasing intensity from 12 to 48 hr, such that it becomes a dominant feature of the discriminating loading. Moreover, the intensity of the 1003 cm^{-1} (Phe) band reduces significantly, while there is a clear broadening of the Amide I band (1550-1700 cm^{-1}). The intensities of the nucleic acid (785 cm^{-1}) and RNA (810cm^{-1}) bands increase further for 24 hr exposure, while the protein and lipid bands (1266, 1299 and 1438 cm^{-1}) become more significant as negative features (unexposed cells) of PC1. The further increase in the intensity of the band at 785 cm^{-1} can be attributed to disruption of membrane structures and release of DNA into the cytoplasm[66].

When cells were exposed to PS-NH_2 for 48 hrs, the exposed cells are differentiated from unexposed cells according to their nucleic acid content, as the bands at 785 and 810 cm^{-1} are observed in the positive features of the loading 1. The band at 1003 cm^{-1}, which indicates the presence of Phe, becomes inverted for the 48 hr exposure. Moreover, the bands at 1299 and 1438 cm^{-1} become dominant in the negative features of the loading 1. The change in the lipid bands can be attributed to further decomposition of lipid structures in cell upon longer exposure. Also, the band at 1268 cm^{-1} appears for this exposure time in the negative features, which indicates a change in the conformational structures of the proteins. The contribution of the Amide I band at 1658 cm^{-1} has become inverted following 48 hr particle exposure. The inverted bands on loading 1 of PC can be attributed to less abundance of proteins and lipids in particle exposed cells.

The spectra of the cytoplasm of PS-NH_2 exposed cells are mainly differentiated from unexposed cells by the intensities of the bands at 785 and 810 cm^{-1}. Moreover, another significant change is observed in the Amide I region of proteins, with increasing exposure time. In order to monitor spectral changes in the Amide I region, the Amide I band (1550-1700 cm^{-1}) was analysed separately in detail. Oxidative stress in a cell causes damage in protein structures and changes the protein secondary structure and tertiary conformation. The changes in protein conformations are reflected in the Amide I region of the Raman spectrum. With increasing exposure time, a broadening and shift is observed in the Amide I band. The Amide I band represents the different secondary structures of the proteins, such as α-helix, ß-sheet, loops[67], and the broadening or shift in Amide I band can be attributed to a change in secondary structure of proteins as a result of oxidative stress.

The Amide I region of proteins in the cytoplasm of PS-NH_2 exposed cells and changes in the bands upon particle exposure are detailed in Figure 6 and Table 1, for different exposure times (I-V) from 4 to 48 hr. The loadings of PC1 of cytoplasm of unexposed and exposed

cells were used and peak fitting was carried out for all exposure times, using LabSpec Software. As seen in Figure 6, the band at 1602 cm^{-1}, which indicates the presence of Phe, is observed for all exposure times, and a change in the total area of the band is observed as a function of time. The band area increases from 0.51 to 1.88, from 4 to 12 hr exposure, but then decreases to 0.34 for 24 hr exposure. Following 48 hr exposure, this band has totally disappeared from the positive features of loading 1. For the first 4 hr particle exposure, both α-helix and ß-sheet structures of protein are observed. However, with increasing exposure time, α-helix structures become dominant and the bands related to the presence of ß-sheet structure disappear (1674 and 1679 cm^{-1}). Thus, with increasing exposure, the Amide I band becomes dominated by α-helix bands, resulting in an apparent shift to lower wavenumbers up to 24 hr exposure. When cells are exposed to the PS-NH_2 for 48 hrs, the Amide I band becomes completely inverted and a sharp band at 1658 cm^{-1}(Amide I, α-helix) is observed in the negative features of the loading 1 [48-50].

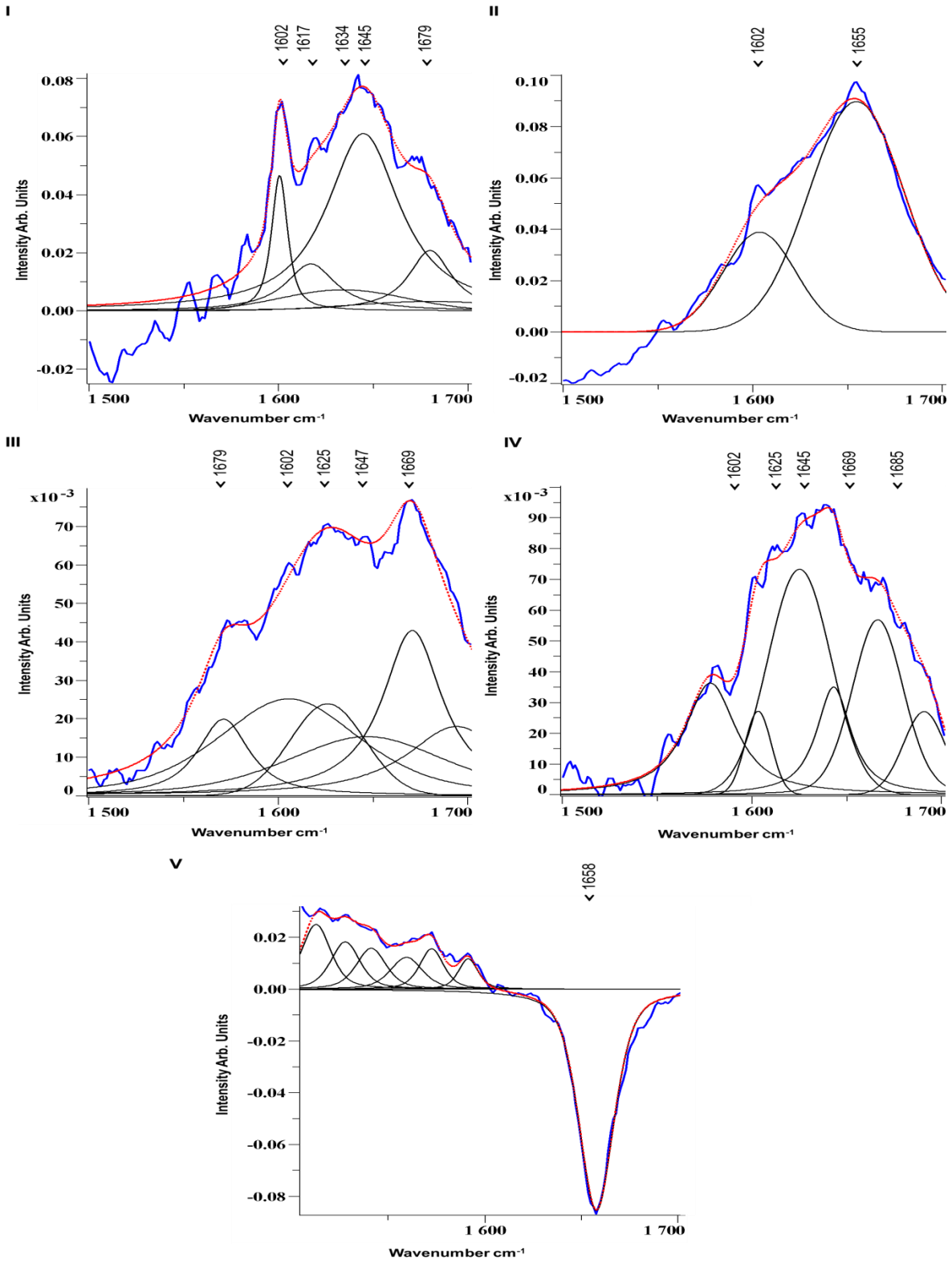

Figure 6. Comparison of the changes in the Amide I region of loading 1 for 4 (I), 8 (II), 12 (III), 24 (IV) and 48 (V) hrs. The loadings and sum of the bands after fitting are indicated

with blue and red lines, respectively. Each individual fitted band is represented by black lines. Peak positions are indicated on the top of the fitted figures.

Table 1. Assignments of Raman Bands of proteins in Amide I Region[47-49,68].

		Band Positions (1550-1700 cm^{-1})	**Band Assignments**
PS-NH_2 Exposed Cells	**4 hour**	1602	Phe
		1618	Trp, Tyr (δ(C=C) stretch.)
		1634	Amide I (Both α-helix and ß sheet)
		1645	Amide I (α-helix)
		1679	Amide I (ß sheet)
	8 hour	1602	Phe
		1655	Amide I (α-helix)
	12 hour	1569	Trp (Indole Ring)
		1602	Phe
		1625	Trp
		1647	Random coils
		1669	Amide I (α-helix)
	24 hour	1582	Phe
		1602	Phe
		1625	Trp
		1645	α-helix
		1669	Amide I (C=O)
		1685	Amide I (disordered structure; non hydrogen bonded)
	48 hr	1658	Amide I (inverted)

Time and dose dependent cytotoxicity can be seen as a 3D response surface rather than a 2D curve, due to the variance of molecular determinants forming overall cytotoxicity[41]. Thus, sublethal concentrations can elicit a similar effect to higher concentrations at different timepoints. Figure 7 shows the comparison of loading 1 of PC of cytoplasm of unexposed and exposed cells for cytoplasm for 8hr exposure 10 μM and 48hr exposure 2.5 μM PS-NH_2. Both loadings show similar positive (exposed cells) and negative features (unexposed cells), with the possible exception of the band at 810 cm^{-1} which indicates the presence of accumulated noncoding RNA in the cytoplasm. This difference can be explained by the more acute toxic effect of repression of translation of mRNA of higher exposure doses. More molecular determinants of toxicity are manifest for the nucleic acid constituents for all exposure times, although more prominantly for high doses and long exposure times. For this reason, the difference in the bands related to nucleic acids can be attributed to changing amounts of molecular determinants. Compared to their controls, exposed cells showed lower contributions of protein and lipids, which can be attributed to damage to these biochemical constituents in particle exposed cells due to oxidative attack.

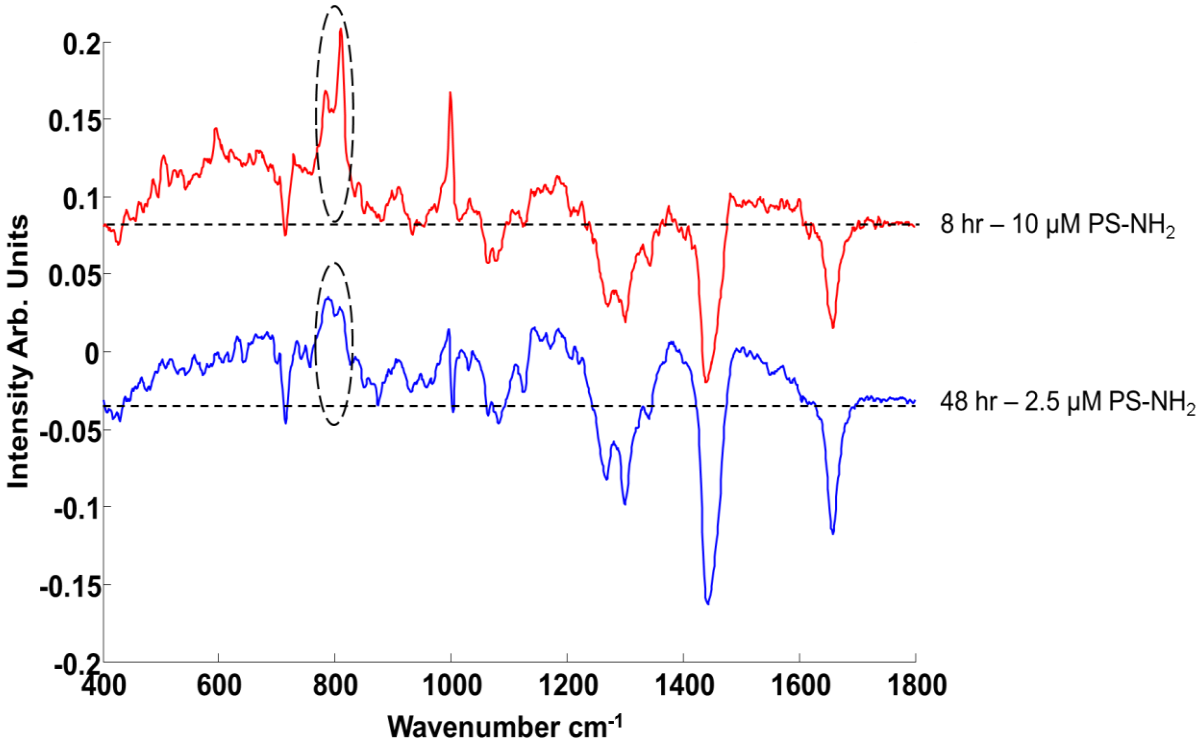

Figure 7. Comparison of the Loading 1 of PCs of cytoplasm for exposed and unexposed cells after 8hr exposure to 10 μM (red) and 48hr 2.5 μM (blue) PS-NH_2. Positive and negative features of the loadings relate to exposed and unexposed cells, relatively. The significant differences between the loadings are indicated with black circles. Loadings are offset for clarity. The dotted line represents the zero '0' point for each loading.

As shown in Figure 2, comparatively fewer changes are observable in the spectral signature of the nucleus and nucleolus, as might be expected, given the uptake and trafficking of the PS-NH_2 is through the cytoplasm, over a period of up to 24 hrs. No localisation of PS-HN_2 nanoparticles in the nucleus has been reported and, indeed, it has been seen that neutral PS nanopatricles are stored in lysosomal vesicles over several passages of the cells[33,69]. Nevertheless, as shown in Figure 8, the mean difference spectrum of the nuclear region does show indications of reduced contributions of nucleic acids at 785 and 810 cm^{-1}, after 24 hr

exposure, consistent with leakage of nuclear material into the cytoplasm after the onset of apoptosis. This is also consistent with the larger increase of nucleic acid features in cytoplasm of PS-NH_2 exposed cells after 24 hr exposure (Figure 5.II).

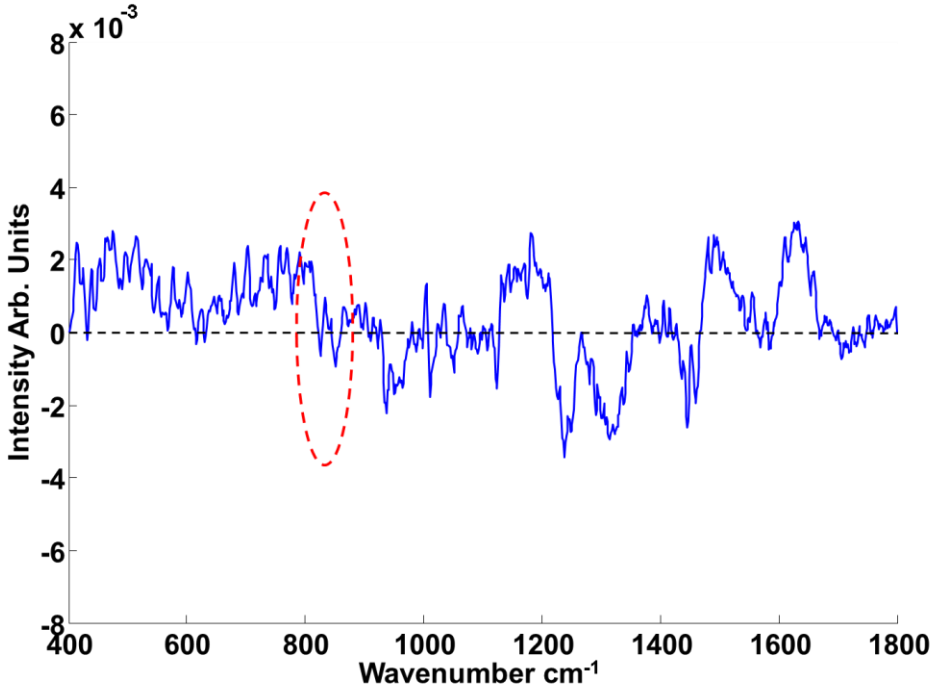

Figure 8. Difference spectrum of nucleus of PS-NH_2 exposed cells and unexposed cells obtained by subtraction of mean spectra of 24 hr PS-NH_2 exposed cells from mean spectra of unexposed cells.

In the case of exposure to the PS-NH_2, the most significant changes are observed in the cytoplasm, as expected due to the uptake mechanism and cellular trafficking of the PSNH_2. The uptake mechanism by endocytosis and subsequent cellular trafficking initiates a series of molecular events and hence molecular determinants of the cytotoxicity. In endocytosis, toxic PS-NH_2 particles are carried to lysosomes by endosomes resulting in lipidosis, lysosomal membrane rupture and ROS in the cytosolic region. The mitochondria of the particle exposed cells are affected as a result of cytosolic changes and mediate the release of pro-inflammatory factors as signals of cytotoxicity. On the other hand, for example doxorubicin, commonly

used anti-cancer chemotherapy drug, is taken into cells by passive diffusion and targets the nuclear region directly. The cytotoxic effects are manifest initially in the nuclear and nucleolar regions of the cell, and only later in the cytoplasm[16]. The process is inverse for PS-NH_2, whereby the toxic effects of the particles are initially seen in the cytoplasmic region for shorter exposure times, although changes in the nuclear area may be more significant in chronic exposures, and linked with genotoxic effects.

In this study, the cytoplasmic changes relating to molecular events upon particle exposure due to the uptake mechanism and cellular trafficking the PS-NH_2, have been evaluated in a dose and time dependent manner, using Raman spectroscopy. The established initial response of oxidative stress is not evident in the spectral response, however. ROS such as hydrogen peroxide (H_2O_2), superoxide anion ($O_2^{-\cdot}$) and hydroxyl radicals ($HO^{\cdot}$) are known to be Raman inactive and, in addition, they are consumed rapidly after initial generation[46,70]. Nevertheless, although the molecular signatures of ROS are not possible to identify with Raman spectroscopy, the signatures of the resultant oxidative stress can be monitored via the signatures of the changes in biochemical constituent of the cells. Oxidative stress in the cytoplasm triggers a complex cascade of events which can include mitochondrial membrane potential decay, caspase activation, apoptosis and ultimately cell death. For a more extensive discussion of the responses, see for example references 29 and 41. The Raman spectral biomarkers of ROS formation, lysosomal damage and biochemical composition changes upon nanoparticle exposure are identified and the most dominant features changing inside the cytoplasm of the cells upon particle exposure are determined to be the bands at 785 and 810 cm^{-1} which can be attributed to nucleic acids inside the cytosol. It is notable, however, that the spectral changes are dominated by the 785 and 810 cm^{-1} bands, rather that the whole spectrum of RNA or DNA[71], suggesting that the spectral signature is due to conformational changes in the nucleic acid structures due to change in the environment rather than

production or consumption of the nucleic material. Especially for sub-lethal doses of PS-NH_2, some contributions are observed to the spectra of cells which indicate a higher protein content compared to control cells. Cells use a recovery mechanism to stabilize the increased ROS levels inside the cells upon exposure to a toxicant[46]. Increased production of enzymes such as superoxide dismutase, catalase, glutathione peroxidase, glutathione reductase, causes an increase in protein related bands. For this reason, the changes in cytosolic acids followed by increased protein profile can be attributed to increased ROS levels and the Raman profile can be used as a Nanotoxicological assay biomarker for a wide variety of nanomaterials.

In comparison with the responses of the classical cytotoxic assays, (Figure 1.II), significant spectral changes are observed over a dose range (from 2.5 to 10 μM), in which MTT shows no change, but AB shows significant change. These spectroscopic changes are therefore better correlated with AB, consistent with an interpretation of origin in cytosolic RNA which subsequently accumulates around the mitochondria. The changes in 1299 and 1438 cm^{-1} bands, which are associated with the later stage toxic response and become inverted after 12 hr particle exposure with an increasing intensity in the negative features of the loading 1, may be better correlated with the MTT response and therefore mitochondrial decay (Figure 5.2). Mitochondrial ROS production can cause significant oxidative stress, damaging protein and lipid structures and mediating the release of factors to initiate the apoptotic process.

Spectral changes, as elucidated by PCA, are complex combinations of contributions of the multitude of biomolecules involved in the cellular responses. However, the combination signature shows consistency in its evolution as a function of time and dose, and correlates well with the known cytotoxic responses. Therefore, not individual spectra, but signatures at 785 cm^{-1} (either RNA or DNA), 810 cm^{-1} (RNA), 1299 cm^{-1} (lipids) and 1435 cm^{-1} (lipids) and proteins Amide I (1550-1700 cm^{-1}) region can be a guide to nanotoxicological screening.

Conclusion

Classical colorometric cytotoxicological assays monitor a single endpoint by which the cellular response to a toxicant is quantified in terms of the IC_{50}. The response is, however, a complex cascade of events, and different assays can report significantly different viability results, and yield little information about the mechanisms of response. The use of a label-free and rapid technique which provides multiparametric information about the changes in the biomolecular structures such as proteins, lipids and nucleic acids following exposure to a toxicant can accelerate the toxicological screening of nanomaterials. This study has identified spectral signatures which are correlated with nanoparticle exposure dose and time, and therefore the known mechanisms of cellular response and toxicity, demonstrating the potential of Raman spectroscopy as a label-free technique to provide multi-parametric information about the biomolecular changes upon a toxicant exposure. It is demonstrated that spectral profiles of the particle exposed cells can be used to track the fingerprint of the molecular responses. Time and dose dependent cytotoxic responses and their reflection to the biochemical fingerprint of the cells can be monitored by using Raman spectroscopy in a progressive way. For all exposure times and doses, the most prominent Raman spectral marker, reflecting the cytotoxic response to exposure to model PS-NH_2 nanoparticles, is found to be the bands at 785 and 810 cm^{-1} in the cytoplasm, reflecting changes in cytoplasmic nucleic acid content. Notably, this response is not normally identified by conventional cytotoxicity assays. The concomitant and subsequent changes in the intensity of the bands corresponding to proteins (Amide I region (1550-1700 cm^{-1}) and lipids (1229 and 1438 cm^{-1}) can also be used to determine toxic effect of nanoparticles. The use of Raman spectroscopy helps to corroborate and further elucidate the mechanism of action of the nanoparticles within

cells and Raman cytotoxicity spectral-markers identified for model nanoparticles can potentially be used to screen for the mode of action and degree of toxicity of novel nanoparticles, in a single label-free assay.

Acknowledgement

This work was supported by Science Foundation Ireland Principle Investigator Award 11/PI/1108.

References

1. Consumer Products Inventory, at http://www.nanotechproject.org/cpi/, (accessed June 2016).

2. G. Oberdörster, E. Oberdörster and J. Oberdörster, *Environ Health Perspect.*, 2005, **113**, 823-839.

3. T. J. Webster, *Int J Nanomedicine*, 2006, **1**, 115–116.

4. K. Donaldson, V. Stone, C. L. Tran, W. Kreyling and P. J. Borm, *Occup. Environ. Med.*, 2004, **61**, 727-728.

5. OECD (2013) OECD Guidelines for the Testing of Chemicals, http://www.oecd.org/chemicalsafety/testing/oecdguidelinesforthetestingofchemicals.htm, (accessed December 2015).

6. W. T. Godbey, K. K. Wu and A. G. Mikos, *Proc. Natl. Acad. Sci. U.S.A.*, 1999, **96**, 5177–5181.

7. G. Tosi, B. Bortot, B. Ruozi, D. Dolcetta, M. A. Vandelli, F. Forni and G. M. Severini, *Curr Med Chem*, 2013, **20**, 2212–2225.

8. H. J. Byrne, G. Sockalingum and N. Stone, in *Biomedical Applications of Synchrotron Infrared Microspectroscopy*, ed. D. Moss, Royal Society of Chemistry, RCS Analytical Spectroscopy Monographs, Cambridge, no. 11, 2011, 4, 105-142.

9. J. R. Ferraro and K. Nakamoto, *Introductory Raman Spectroscopy*, Academic Press, Orlando, 1994.

10. A. G. Walton, M. J. Deveney and J. L. Koenig, *Calcified Tissue Research*, 1970, **6**, 162-167.

11. G. J. Puppels and J. Breve, in *Biomedical Applications of Spectroscopy*, ed. R. J. H. Clark and R. E. Hester, Wiley, Chichester, 1996, 1, 1-47.

12. F. Bonnier, F. Petitjean, M. J. Baker and H. J. Byrne, *Journal of Biophotonics*, 2014, **7**, 167-179.

13. F. Bonnier, A. Mehmood, P. Knief, A. D. Meade, W. Hornebeck, H. Lambkin, K. Flynn, V. McDonagh, C. Healy, T. C. Lee, F. M. Lyng and H. J. Byrne, *Journal of Raman Spectroscopy*, 2011, **42**, 888–896.

14. J. Dorney, F. Bonnier, A. Garcia, A. Casey, G. Chambers, and H. J. Byrne, *Analyst*, 2012, **137**, 1111-1119.

15. E. Efeoglu, M. Keating, J. McIntyre, A. Casey and H. J. Byrne, *Anal. Methods*, 2015, **7**, 10000–10017.

16. Z. Farhane, F. Bonnier, A. Casey and H. J. Byrne, 2015, *Analyst*, **140**, 4212-4223.

17. Z. Farhane, F. Bonnier, M. A. Maher, J. Bryant, A. Casey and H. J. Byrne, *J Biophotonics*, 2016, 1–15 / DOI 10.1002/jbio.201600019.

18. H. Nawaz, F. Bonnier, P. Knief, O. Howe, F. M. Lyng, A. D. Meade and H. J. Byrne, *Analyst*, 2010, **135**, 3070-3076.

19. H. Nawaz, F. Bonnier, A. D. Meade, F. M. Lyng and H. J. Byrne, *Analyst*, 2011, **136**, 2450-2463.

20. H. Nawaz, A. Garcia, A. D. Meade, F. M. Lyng and H. J. Byrne, *Analyst*, 2013, **138**, 6177-6184.

21. C. A. Owen, J. Selvakumaran, I. Notingher, G. Jell, L. L. Hench and M. M. Stevens, *J Cell Biochem*, 2006, **99**, 178-186.

22. A. Zoladek, F. C. Pascut, P. Patel and I. Notingher, *Journal of Raman Spectroscopy*, 2011, **42**, 251–258.

23. T. Chernenko, C. Matthäus, L. Milane, L. Quintero, M. Amiji and M. Diem, *ACS nano*, 2009, **3**, 3552–3559.

24. M. E. Keating, F. Bonnier and H. J. Byrne, *Analyst*, 2012, **137**, 5792–5802.

25. P. Knief, C. Clarke, E. Herzog, M. Davoren, F. M. Lyng, A. D. Meade and H. J. Byrne, *Analyst*, 2009, **134**, 1182-1191.

26. S. Anguissola, D. Garry, A. Salvati, P. J. O'Brien and K. A. Dawson, *PLoS ONE*, 2014, **9**, e108025.

27. O. Lunov, T. Syrovets, C. Loos, J. Beil, M. Delacher, K. Tron, G. U. Nienhaus, A. Musyanovych, V. Mailänder, K. Landfester and T. Simmet, *ACS Nano*, 2011, **5**, 1657-1669.

28. O. Lunov, T. Syrovets, C. Loos, G. U. Nienhaus, V. Mailänder, K. Landfester, M. Rouis and T. Simmet, *ACS Nano*, 2011, **5**, 9648-9657.

29. T. Xia, M. Kovochich, M. Liong, J. I. Zink and A. E. Nel, *ACS Nano*, 2008, **2**, 85-96.

30. P. Ruenraroengsak, P. Novak, D. Berhanu, A. J. Thorley, E. Valsami-Jones, J. Gorelik, Y. E. Korchev and T. D. Tetley, *Nanotoxicology*, 2012, **6**, 94-108.

31. F. Wang, L. Yu, M. P. Monopoli, P. Sandin, E. Mahon, A. Salvati and K. A. Dawson, *Nanomedicine*, 2013, **9**, 1159–1168.

32. L. Treuel, X. Jiang and G. U. Nienhaus, *J R Soc Interface*, 2013, **10**, 20120939.

33. K. Shapero, F. Fenaroli, I. Lynch, D. C. Cottell, A. Salvati and K. A. Dawson, *Mol BioSyst*, 2011, **7**, 371–378.

34. Q. Mu, N. S. Hondow, L. Krzemiński, A. P. Brown, L. J. Jeuken and M. N. Routledge, *Part Fibre Toxicol*, 2012, **9**, 29.

35. M. G. Bexiga, J. A. Varela, F. Wang, F. Fenaroli, A. Salvati, I. Lynch, J.C. Simpson and K. A. Dawson, *Nanotoxicology*, 2011, **5**, 557-567.

36. M. Miljkovic, T. Chernenko, M. J. Romeo, B. Bird, C. Matthaus and M. Diem, *Analyst*, 2010, **135**, 2002-2013.

37. M. V. Berridge, P. M. Herst and A. S. Tan, *Biotechnol Annu Rev*, 2005, **11**, 127-152.

38. S. N. Rampersad, *Sensors*, 2012, **12**.

39. E. Vega-Avila and M. K. Pugsley, *Proc West Pharmacol Soc*, 2011, **54**, 10-14.

40. D. Ragnvaldsson, R. Berglind, M. Tysklind and P. Leffler, *Ambio*, 2007, **36**, 494-501.

41. M. A. Maher, P. C. Naha, S. P. Mukherjee and H. J. Byrne, *Toxicology In Vitro*, 2014, **28**, 1449-1460.

42. M. J. White, M. J. DiCaprio and D. A. Greenberg, J *Neurosci Methods*, 1996, **70**, 195-200.

43. J. O'Brien, I. Wilson, T. Orton and F. Pognan, *Eur J Biochem*, 2000, **267**, 5421-5426.

44. T. Mosmann, *J Immunol Methods*, 1983, **65**, 55-63.

45. S. P. Mukherjee, N. O'Claonadh, A. Casey and G. Chambers, *Toxicol In Vitro*, 2012, **26**, 238-251.

46. L. Casteilla, M. Rigoulet and L. Penicaud, *IUBMB Life*, 2001, **52**, 181–188.

47. T. P. Pobezhimova and V. K. Voinikov, *Membr Cell Biol*, 2000, **13**, 595–602.

48. I. Notingher, S. Verrier, S. Haque, J. M. Polak and L. L. Hench, *Biopolymers*, 2003, **72**, 230–240.

49. I. Notingher and L. L. Hench, *Expert Rev Med Devices*, 2006, **3**, 215–234.

50. Z. Movasaghi, S. Rehman and I. U. Rehman, *Applied Spectroscopy Reviews*, 2007, **42**, 493-541.

51. E. Fröhlich, C. Meindl, E. Roblegg, B. Ebner, M. Absenger and T. R Pieber, *Fibre Toxicol*, 2012, **9**, 26.

52. C. Loos, T. Syrovets, A. Musyanovych, V. Mailänder, K. Landfester, G. U. Nienhaus and T. Simmet, *Beilstein Journal of Nanotechnology*, 2014, **5**, 2403-2412.

53. M. Ekkapongpisit, A. Giovia, C. Follo, G. Caputo and C. Isidoro, *Int J Nanomedicine*, 2012, **7**, 4147–4158.

54. E. W. Small and W.L. Peticolas, *Biopolymers*, 1971, **10**, 69-88.

55. G. J. Thomas, G. C. Medeiros and K. A. Hartman, *Biochemical and Biophysical Research Communications*, 1971, **44**, 587-592.

56. A. Ghita, F. C. Pascut, M. Mather, V. Sottile and I. Notingher, *Anal Chem*, 2012, **84**, 3155-3162.

57. P. Ruenraroengsak and T. D. Tetley, *Part Fibre Toxicol*, 2015, **12**, 19.

58. T. Xia, M. Kovochich, J. Brant, M. Hotze, J. Sempf, T. Oberley, C. Sioutas, J. I. Yeh, M. R. Wiesner and A. E. Nel, *Nano Lett*, 2006, **6**, 1794-1807.

59. M. Saikia, D. Krokowski, B. J. Guan, P. Ivanov, M. Parisien, G. F. Hu, P. Anderson, T. Pan and M. Hatzoglou, *J Biol Chem*, 2012, **287**, 42708–42725.

60. S. Yamasaki, P. Ivanov, G. F. Hu and P. Anderson, *J Cell Biol*, 2009, **185**, 35–42.

61. A. Czech, S. Wende, M. Mörl, T. Pan and Z. Ignatova, *PLoS Genet*, 2013, **9**, e1003767.

62. H. Lüllmann, R. Lüllmann-Rauch and O. Wassermann, *Biochem Pharmacol*, 1978, **27**, 1103-1108.

63. N. D. Sonawane, J. R. Thiagarajah, and A. S. Verkman, *J Biol Chem*, 2002, **277**, 5506–5513.

64. D. Drenckhahn, L. Kleine and R. Lüllmann-Rauch, *Lab invest*, 1976, **35**, 116-123.

65. A. Asokan and M. J. Cho, *J Pharm Sci*, 2002, **91**, 903–913.

66. S. Elmore, *Toxicol Pathol*, 2007, **35**, 495–516.

67. B. H. Stuart, *Biological Applications of Infrared Spectroscopy*, ACOL Series, Wiley, Chichester, UK, 1997.

68. A. Rygula, K. Majzner, K. M. Marzec, A. Kaczor, M. Pilarczyk and M. Baranska, *Journal of Raman Spectroscopy*, 2013, **44**, 1061–1076.

69. A. Salvati, C. Åberg, T. dos Santos, J. Varela, P. Pinto, I. Lynch and K. A. Dawson, *Nanomedicine NBM*, 2011, **7**, 818-826.

70. S. P. Mukherjee and H. J. Byrne, *Nanomedicine NBM*, 2012, **9**, 202-211.

71. F. Bonnier, P. Knief, B. Lim, A. D. Meade, J. Dorney, K. Bhattacharya, F. M. Lyng and H. J. Byrne, *Analyst*, 2010, **135**, 3169-3177.